Research Article

Generation and manipulation of chiral terahertz waves in the three-dimensional topological insulator Bi₂Te₃

Haihui Zhao,[a,†] **Xinhou Chen,**[b,†] **Chen Ouyang,**[c,d,†] **Hangtian Wang** [a,e,†] **Deyin Kong,**[b] **Peidi Yang,**[b] **Baolong Zhang,**[c,d] **Chun Wang,**[c,d] **Gaoshuai Wei,**[c,d] **Tianxiao Nie,**[a,e,*] **Weisheng Zhao,**[a,e,*] **Jungang Miao,**[b] **Yutong Li,**[c,d] **Li Wang,**[c,*] **and Xiaojun Wu**[b,f,*]

[a]Beihang University, Fert Beijing Institute, Advanced Innovation Center for Big Data and Brain Computing, School of Microelectronics, Beijing, China
[b]Beihang University, School of Electronic and Information Engineering, Beijing, China
[c]Chinese Academy of Sciences, Institute of Physics, Beijing National Laboratory for Condensed Matter Physics, Beijing, China
[d]University of Chinese Academy of Sciences, School of Physical Sciences, Beijing, China
[e]Beihang University, Beihang-Goertek Joint Microelectronics Institute, Qingdao Research Institute, Qingdao, China
[f]Wuhan National Laboratory for Optoelectronics, Huazhong University of Science and Technology, China

Abstract. Arbitrary manipulation of broadband terahertz waves with flexible polarization shaping at the source has great potential in expanding numerous applications, such as imaging, information encryption, and all-optical coherent control of terahertz nonlinear phenomena. Topological insulators featuring unique spin-momentum–locked surface state have already exhibited very promising prospects in terahertz emission, detection, and modulation, which may lay a foundation for future on-chip topological insulator-based terahertz systems. However, polarization-shaped terahertz emitters based on topological insulators with an arbitrarily manipulated temporal evolution of the amplitude and the electric-field vector direction have not yet been explored. We systematically investigated the terahertz radiation from topological insulator Bi₂Te₃ nanofilms driven by femtosecond laser pulses and successfully realized the generation of efficient chiral terahertz waves with controllable chirality, ellipticity, and principal axis. The convenient engineering of the chiral terahertz waves was interpreted by a photogalvanic effect (PGE)-induced photocurrent, while the linearly polarized terahertz waves originated from linear PGE-induced shift currents. Our work not only provides further understanding of femtosecond coherent control of ultrafast spin currents but also describes an effective way to generate spin-polarized terahertz waves at the source.

Keywords: spin-polarized terahertz; manipulation; topological insulator; photogalvanic effect.

1 Introduction

Spin-polarized terahertz waves with twisted electric- and magnetic-field directions and temporal evolution of the amplitudes have been widely utilized for non-thermal and selective excitation of electron spins, resulting in the discovery of the spin-galvanic effect,[1] the manipulation of terahertz nonlinear phenomena,[2] and optical spin injection in novel materials.[3–5] Recently, Mashkovich et al.[6] found that linearly polarized terahertz waves can nonlinearly excite gigahertz spin waves in antiferromagnetic FeBO₃ via terahertz field-induced inverse Cotton–Mouton effect. However, the inverse Faraday effect excited by circularly polarized terahertz waves has not yet been experimentally demonstrated, despite many theoretical predictions reported.[7] Therefore, spin-polarized terahertz waves are

*Address all correspondence to Xiaojun Wu, xiaojunwu@buaa.edu.cn; Tianxiao Nie, nietianxiao@buaa.edu.cn; Weisheng Zhao, weisheng.zhao@buaa.edu.cn; Li Wang, wangli@aphy.iphy.ac.cn

†These authors contributed equally.

essential for revealing electron spin-related linear and nonlinear ultrafast phenomena. In addition, spin-polarized terahertz waves naturally carrying chiral properties offer multifaceted spectroscopic capabilities for investigating low-energy macromolecular vibrations in biomaterials, understanding the mesoscale chiral architecture[8] and confidential communication.[9,10] However, the proliferation of terahertz circular dichroism spectroscopy and other applications is impeded by the lack of generation and manipulation of chiral terahertz waves.

Conventional polarization shapers working in the terahertz electromagnetic frequency range are mainly segmental waveplates and metasurfaces,[11,12] both of which can be well applied for narrow bandwidth applications and low tolerance of flexible tunability. Various scalar manipulations of terahertz waves have been demonstrated in poled nonlinear optical crystals[13,14] or even in water[15] and have synthesized different frequencies generated in spatially distributed sources.[16] However, it would be much more elegant if polarization shaping functionality could be vectorized and integrated into the sources. Currently, there are already several such kinds of vector-manipulated polarized terahertz sources.[17–21] For example, femtosecond laser amplifier pumped air plasma, when intensively tuning the phase delay and the pump pulse polarization between two different pump pulse colors, can enable the opportunity to obtain arbitrarily shaped terahertz polarizations.[17] Furthermore, terahertz polarization pulse shaping with arbitrary field control has also been demonstrated by optical rectification of a laser pulse whose instantaneous intensity and polarization state are flexibly controlled by an optical pulse shaper.[18] Recently, elliptically and circularly polarized terahertz waves have been realized in W/CoFeB/Pt heterostructures through deliberately engineering the applied magnetic-field distribution and the cascade emission method, respectively.[19,20] In a NiO single crystal, double-pulse excitation has also been used to vectorially control magnetization by radiating spin-polarized terahertz waves,[21] in which an electron spin-polarized wave (magnon oscillation) has been purposely vectorially controlled and manipulated. In addition, highly efficient chiral terahertz emission with elliptical polarization states has been obtained from the fascinating topological phase matter, bulk Weyl semimetal TaAs with reflection terahertz emission geometry.[22] Inspired by these pioneering breakthroughs, the question of whether we can utilize the spin freedom of electrons to generate and manipulate spin-polarized terahertz waves has become very interesting.

Three-dimensional topological insulator Bi_2Te_3 single crystals grown on Al_2O_3 substrates not only feature the spin-momentum–locked (topologically protected) surface states but also are adapted for various heterostructures with tunable quantum layers.[23] They are predicted to have the potential for achieving vectorial polarization shaping terahertz sources. The charge current and spin current inside topological insulators are simultaneously excited when being driven by femtosecond laser pulses.[24–28] However, topological insulator-based terahertz emission mechanisms are far more complicated when compared with conventional terahertz emitters. It is clarified that nonlinear effects play a predominant role in the ultrafast terahertz emission process.[29] Nonlinear effects include optical rectification, photogalvanic effect (PGE), and photon drag effect, among which PGE has a strong correlation to electron spin. Thus, there is the feasibility to generate a femtosecond laser helicity-dependent current component resulting in synthesizing chiral terahertz light.
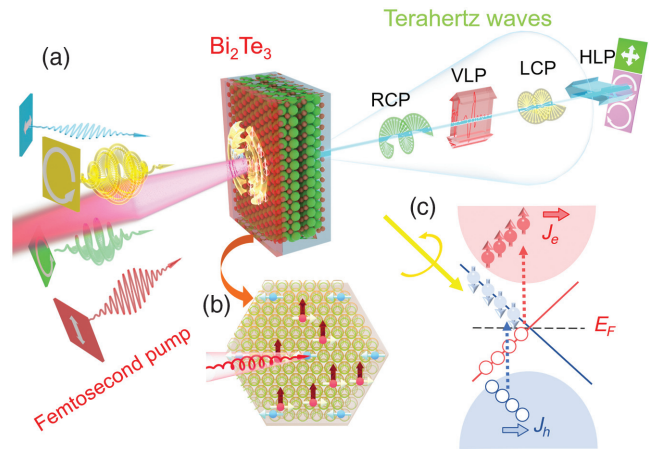

Fig. 1 Schematic diagram of the polarization tunable terahertz emission from Bi_2Te_3. (a) Femtosecond laser pulses, horizontal linear polarization (HLP), vertical linear polarization (VLP), left-handed circular polarization (LCP), and right-handed circular polarization (RCP), are incident onto the topological insulator Bi_2Te_3 and produce polarization tunable terahertz waves. (b) Macroscopic helicity-dependent photocurrent and only unidirectional spin current can be generated. (c) Microscopic electronic transition under circularly polarized laser pulse illumination (Video 1, MP4, 15.5 MB [URL: https://doi.org/10.1117/1.AP.2.6.066003.1]).

In this work, we systematically studied terahertz emission from Bi_2Te_3 nanofilms with various thicknesses grown on Al_2O_3 substrates excited by femtosecond laser pulses. Through elaborately controlling the pump laser pulse polarization, its incident angle, and the sample azimuthal angle, we not only successfully realized efficient linear polarization tunable terahertz radiation but also obtained high-quality chiral terahertz waves, as shown in Fig. 1(a). In addition, we also demonstrated arbitrary manipulation of the ellipticity and chirality of the emitted terahertz waves from topological insulators. Based on the radiated terahertz characteristics, which originated from the helicity-dependent photocurrent component featuring the spin selectivity in the surface state [Fig. 1(b)] and other components in the bulk state[30] [Fig. 1(c)], we provide a phenomenological PGE-based interpretation for the polarization tunable terahertz radiation mechanism. Such polarization-shaped topological insulator-based terahertz source can be used for terahertz circular dichroism spectroscopy, terahertz secure wireless communication, and electron spin correlated coherent excitation and manipulation investigations.

2 Linearly Polarized Terahertz Emission

2.1 Experimental Results

In this experiment, we employed a commercial Ti:sapphire laser oscillator delivering nJ magnitude pulse energy with a central wavelength of 800 nm, a pulse duration of 100 fs, and a repetition rate of 80 MHz. The pump laser polarization was varied by inserting either a half-wave plate or a quarter-wave plate. The radiated terahertz polarization was probed by a polarization-resolved electro-optic sampling detection method. The topological insulator samples were grown by molecular beam epitaxy (MBE), and their lattice structures and the characterizations

can be found in Supplementary Note 1 and Fig. S1 in the Supplementary Material.

First, we examined the sample azimuthal angle-dependent terahertz radiation polarization properties to unveil the radiation mechanism in topological insulators driven by femtosecond laser pulses. For the p-polarized pump laser at nearly normal incidence, as shown in Fig. 2(a), the radiated terahertz signal from 10-nm-thick Bi_2Te_3 was $\sim 1/20$ compared with that from 1-mm-thick ZnTe (see Supplementary Note 2 and Fig. S2 in the Supplementary Material) and with ~ 100 dynamic range, which manifests its feasibility for terahertz spectroscopy. The radiated terahertz waves were always linearly polarized with a three-fold rotation angle depending on the sample azimuthal angle, as shown in Figs. 2(b) and 2(c). For the pump-fluence-dependence results [Fig. 2(d)], the terahertz signals of different thickness all exhibited a linear increasing tendency, indicating that the terahertz radiation mechanism under the linear-polarization laser pump was predominated by a second-order nonlinear effect.

2.2 Mechanism of Linearly Polarized Terahertz Emission

Nonlinear effect radiation mechanisms include optical rectification (OR), photon-drag effect (PDE), and PGE. To evaluate the relative importance of optical rectification in our experiment, we compared the emitted terahertz amplitude from the topological insulator sample with that from a ZnTe crystal, which is known for relatively strong optical rectification at the pump wavelength used here. We found that the terahertz signal from topological insulator was almost 3 orders of magnitude larger than that from ZnTe when we normalized the amplitudes by the emitter thicknesses (see Supplementary Note 2 and Fig. S2 in the Supplementary Material). Therefore, we can safely rule out optical rectification as the predominant radiation mechanism.[31] Linear photon-drag effect (LPDE) can be microscopically understood as the linear transfer from photon momentum to electron momentum, which means that when the opposite incident angle was employed, we would obtain opposite polarity of terahertz signals. However, when we varied the incident angles with opposite signs under the p-polarized laser pumping, which was a pure LPDE case, such behaviors neither for $S_x(t)$ nor for $S_y(t)$ were not observed, as described in Supplementary Note 4 and Fig. S4 in the Supplementary Material. Hence, we can further safely remove the LPDE as the primary radiation origin.

Macroscopically, PGE is a second-order nonlinear process occurring in the noncentral symmetric structure. From the microscopic physical picture, PGE can be understood as optical transition on the surface states,[31,32] which can be divided into linear PGE (LPGE) and circular PGE (CPGE). The linear photogalvanic current, also named a shift current, can be explained in that the electron density distribution is spatially shifted from state 1 to state 2 along the Bi–Te bonds [see Fig. 2(e)] when the pump laser pulses illuminate the topological insulator, following a relaxation process such as asymmetric scattering due to the optical electric field.[31] For this mechanism underlying the terahertz emission scenario, we can quantify the behavior on both x and y directions by analyzing the symmetry of the terahertz signals. The three-fold rotational symmetry of signals is in coordination with the space group of the surface and bulk, such that we can write the two-dimensional waveform set $S(t, \varphi)$ as a linear combination of three bases,[31]
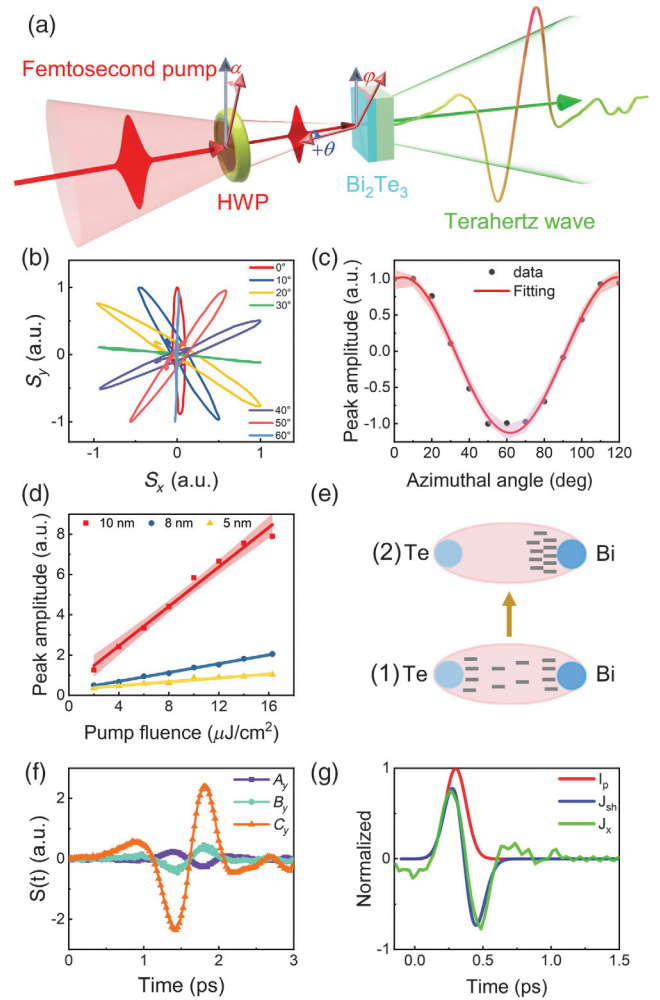

Fig. 2 Linearly polarized terahertz emission and its shift current mechanism. (a) Schematic diagram of the experimental setup for linearly polarized terahertz emission. Linearly polarized laser pump passes through a half-wave plate of angle α and is incident onto the sample emitting linearly polarized terahertz wave. The incident angle of the pump laser, θ; the azimuthal angle of the topological insulator, φ. (b) Far-field polarization trajectories $[S_x(t), S_y(t)]$ of the radiated terahertz waves obtained experimentally from 10-nm-thick Bi_2Te_3 when the pump laser polarization was nearly normal incidence while the sample azimuthal angle was varied. (c) The terahertz peak amplitude of $S_y(t)$ as a function of the azimuthal angle exhibits a 120-deg period. (d) Pump fluence dependence of terahertz peak amplitude from Bi_2Te_3 with different thickness of 5, 8, and 10 nm. (e) Schematic of the shift current generated from the electron transfer along the Bi–Te bonds. (f) Parameters in the y axis extracted through the symmetry analysis of surface state using Eq. (1). (g) I_p denotes the laser intensity profile. Fitting the shape of the shift current (blue line) to the photocurrent in the material (green line).

$$S(t, \varphi) = A(t) + B(t)\sin(3\varphi) + C(t)\cos(3\varphi). \qquad (1)$$

Thus, these three bases can completely characterize $S(t, \varphi)$. Among the three coefficients, $B(t)$ and $C(t)$ represent the pure LPGE-dependent components, while $A(t)$ represents a direct current component, which might be ascribed to a thermal

current caused by the thermal potential gradient when the sample was under pumping. From the extracted coefficients in the y axis, as shown in Fig. 2(f) (coefficients in the x axis can be found in Supplementary Note 4 and Fig. S5 in the Supplementary Material), it is obvious that the thermal current contributes much less than the shift current. Therefore, the thermal effect in our Bi_2Te_3 material under excitation can be safely ignored. We only need to consider the shift current in the generation process of the linearly polarized terahertz wave scenario.

As for a more profound insight about the shift current generated under the short-pulse excitation, this process results in a step-like charge displacement $\Delta x_{sh}\Theta(t)$, where Δx_{sh} is the spatial displacement of the electron density, $\Theta(t)$ denotes the unit step function, whose temporal derivative is proportional to the shift current J_{sh}. A phenomenological relaxation process such as scattering should also be included so that an exponential decay term with time constant τ_{sh} has to be introduced. Therefore, we obtain the shape of the shift current as follows:

$$J_{sh} \propto \Delta x_{sh} \frac{\partial}{\partial t}\left[\Theta(t)\exp\left(-\frac{t}{\tau_{sh}}\right)\right] * I_p. \qquad (2)$$

The convolution (marked by *) with the laser intensity profile $I_p(t)$ (normalized to unit) accounts for the influence under the process of excitation. This model illustrates that the profile of J_{sh} initially follows the envelope of $I_p(t)$ and subsequently becomes bipolar, as shown in Fig. 2(g) (blue line). Due to the relatively flat response function of $ZnTe$[33] within the low-frequency range (<3 THz), we can semi-quantitatively retrieve the photocurrent (green line) inside the material [see Appendix (Sec. 5) and Supplementary Note 4 and Fig. S6 in the Supplementary Material]. Moreover, to fit the photocurrent through the theoretical model, $I_p(t)$ exhibits an extension of its pulse duration from 140 to 170 fs (red line), and the retrieved photocurrent agrees well with the calculated results among the whole profile. According to the fitting process, we obtain the relaxation time $\tau_{sh} = 22$ fs, which is consistent with that in the previous literature,[31] further proving the validity of the LPGE mechanism under this circumstance. It has been reported that the shift current in Bi_2Te_3 originated from the transient electron transfer along the Bi–Te bonds involving the surface-states-related optical transitions. However, for ultrathin Bi_2Te_3 nanofilms, the coupling between the top and bottom surface opens a gap in the surface state dispersion and, hence, suppresses the surface-states-related optical transitions.[23] Therefore, as shown in Fig. 2(d), the shift current as well as its resulting terahertz emission decreases considerably.

3 Chiral Terahertz Wave Emission and Manipulation

As shown in Fig. 3(a), when the left-handed circularly polarized (LCP) pump light was incident onto the sample at an incident angle around $+20$ deg, and, when we rotated the sample azimuthal angle, elliptically polarized terahertz waves were obtained and showed no significant change when scanning the azimuthal angle φ in Fig. 3(b). To produce circularly polarized terahertz pulses, simultaneously tuning the pump laser polarization and the sample azimuthal angle was necessary. The experimental results are shown in Fig. 3(c). When the sample azimuthal angle was fixed, we can also obtain elliptical terahertz beams with various ellipticities and principal axes. Within
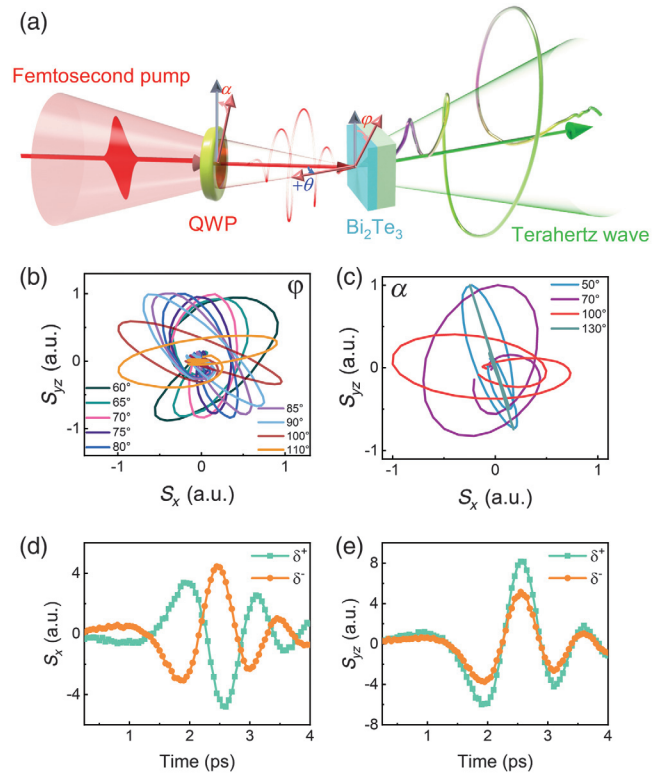

Fig. 3 Generation of elliptically and circularly polarized terahertz beams. (a) Experimental layout for circularly-polarized terahertz wave generation. Linearly polarized laser pump passes through a quarter-wave plate of angle, α, producing elliptically or circularly polarized pump laser beams. The emitted terahertz wave polarization can be elliptical or circular. The incident angle of the pump laser, θ; the azimuthal angle of the topological insulator, φ. (b) Far-field detected elliptically polarized terahertz polarization trajectories when the pump laser polarization was fixed while rotating the sample azimuthal angles. (c) Production of circularly polarized terahertz waves when fixing the azimuthal angle while rotating the quarter-wave plate for the pump laser pulses. (d) Experimentally observed terahertz component $S_x(t)$ polarity reversal depends on the pump laser helicity. (e) Helicity-independent component $S_{yz}(t)$ from Bi_2Te_3. δ^+ and δ^- mean left-handed and right-handed elliptically polarized terahertz, respectively.

expectations, we can manipulate the chirality of the emitted terahertz waves via varying the incident laser helicity. It is obvious that the polarity of emitted terahertz signal along the x direction reversed under illumination of the laser with different chirality [Fig. 3(d)] and sustained the sign along the yz plane [Fig. 3(e)]. Therefore, the generation of pump laser helicity-dependent photocurrents with continuous tuning of the magnitude and polarity is the primary reason for the production of elliptically and circularly polarized terahertz pulses.

To further investigate the helicity-dependent terahertz signal, a terahertz pulse with chirality was manipulated by rotating the quarter-wave plate with an angle α at a fixed incident angle around $+20$ deg. During the α scanning, the terahertz peak values clearly exhibited a 180-deg period [Fig. 4(a)], and the waveform shape along the x axis was very similar to the result in Ref. 24 in the Sb_2Te_3 thin film system. It illustrates the analogies among the family of topological insulators.
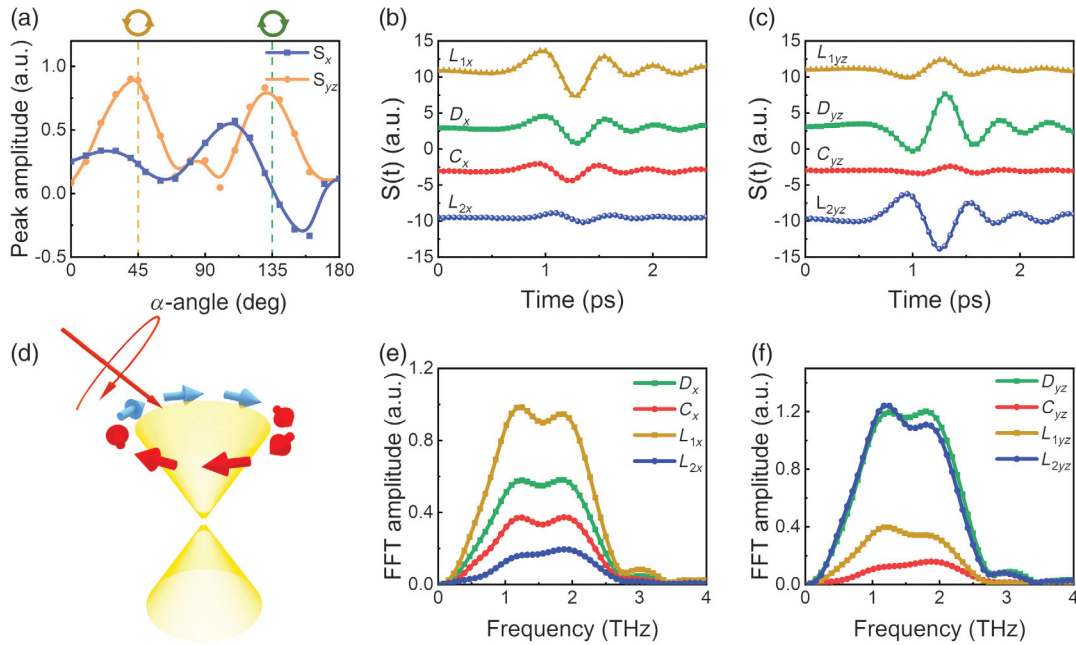
Fig. 4 Macroscopic analysis of PGE. (a) The terahertz peak amplitude of $S_x(t)$ and $S_{yz}(t)$, as a function of the quarter-wave plate angle, respectively. (b) and (c) The time-domain signals for the parameters $C(t)$, $L_1(t)$, $L_2(t)$, and $D(t)$ in the x axis and yz plane extracted using Eq. (3). (d) Spin-momentum-locked states selectively excited by spin-polarized pump laser form unidirectional spin currents. (e) and (f) The corresponding Fourier transformed spectra of the time-domain signals in (b) and (c).

Therefore, based on the geometric structure of the incident laser that was modulated via the quarter-wave plate (Supplementary Note 6 and Fig. S8 in the Supplementary Material), we can write the signal in the following form:[25,26,34]

$$S(t,\alpha) = C(t)\sin(2\alpha) + L_1(t)\sin(4\alpha) + L_2(t)\cos(4\alpha) + D(t). \quad (3)$$

The coefficient $C(t)$ describes the helicity-dependent terahertz radiation that originates from CPGE. $L_1(t)$ denotes the coefficient induced by linearly polarized light, and LPGE may be responsible for it. For terahertz emission in 40-nm Sb$_2$Te$_3$, Yu et al.[34] attributed the origin of $L_2(t)$ to LPDE and experimentally verified that the trend of $L_2(t) + D(t)$ under the variation of the incidence angle θ was in accordance with the trend of pure LPDE for p-polarized laser excitation. However, as aforementioned, LPDE has already been eliminated, so it is not suitable for elucidating this phenomenon. In terms of $D(t)$, there is no uniform statement, and it is still subject to controversial debate. LPGE, drift current out of plane, or photo–Dember effect may be the candidates for this coefficient.

Accordingly, we extracted all coefficients along the x axis and yz plane (see Sec. 2). All data were offset to ensure great clarity, as shown in Figs. 4(b) and 4(c), which show the time-domain trace for every component. The main characteristics are summarized as follows. (i) In magnitude, along the x axis, C_x, L_{1x}, and D_x dominate the main components, while L_{2x} is negligible. They are sorted from the largest to smallest $L_{1x} > D_x > C_x$. Along the yz plane, L_{2yz} and D_{yz} dominate the main components, while L_{1yz} and C_{yz} are negligible. In addition, L_{2yz} and D_{yz} have almost the same magnitude.

(ii) C_x shows similar characteristics to those for L_{1x}. In fast Fourier transformed spectra of C_x and L_{1x} [Figs. 4(e) and 4(f)], they both presented the same spectral shapes, strongly indicating that both C_x and L_{1x} shared the same physical origin and are consistent with previous observation.[25,26,35–38] However, the D_x, L_{2yz}, and D_{yz} terms also presented similar shapes in the frequency domain, and very few works pay attention to the underlying mechanism about these three terms. Ours is the first observation that all five terms resemble each other in nature, and we elucidate this phenomenon in a macroscopic phenomenological PGE-induced photocurrent framework.

Macroscopically, as a second-order nonlinear optical process, the PGE-induced photocurrent vanishes in the bulk region where inversion symmetry exists. Only on the surface where inversion symmetry is broken, the photocurrent induced by PGE can occur. Thus, taking the C_{3v} symmetry into account, in our specific case in which the incident pulse shines on the yz plane, the arbitrary polarized laser pulse-induced photocurrent can be separated to CPGE- and LPGE-induced components (see the derivation in Supplementary Note 6 in the Supplementary Material):

$$j_{\text{CPGE}} = -2\gamma C^2 \begin{pmatrix} \sin 2\alpha \sin \theta \\ 0 \\ 0 \end{pmatrix}, \quad C = \frac{\omega A_0}{2}. \quad (4)$$

The LPGE-induced photocurrent can be written in a compact way, $j_{\text{LPGE}} = \begin{pmatrix} j_x \\ j_y \\ j_z \end{pmatrix}$, and all components are written as

$$j_x = -2C^2(\eta_1 \cos \theta + \eta_2 \sin \theta) \sin 4\alpha, \qquad (5)$$

$$j_y = 2C^2 \left[\eta_1 \left(\frac{1}{2} \cos^2 \theta + \frac{1}{2} \right) - \eta_2 \sin \theta \cos \theta \right] \cos 4\alpha$$
$$+ 2C^2 \left[\eta_1 \left(\frac{3}{2} \cos^2 \theta - \frac{1}{2} \right) - 3\eta_2 \sin \theta \cos \theta \right], \qquad (6)$$

$$j_z = 2C^2 \left[\eta_3 \frac{1}{2} \sin^2 \theta + \eta_4 \left(\frac{1}{2} \cos^2 \theta - \frac{1}{2} \right) \right] \cos 4\alpha$$
$$+ 2C^2 \left[\eta_3 \frac{3}{2} \sin^2 \theta + \eta_4 \left(\frac{1}{2} + \frac{3}{2} \cos^2 \theta \right) \right], \qquad (7)$$

where the incident angle is θ, the rotated angle of the quarter-wave plate is α, and γ and η denote the independent components for CPGE and LPGE tensor elements, respectively.

From the above four PGE-induced photocurrent equations, we can obtain four conclusions. (i) For the incident laser with arbitrary polarization and directions, in addition to the CPGE-induced term $j_{CPGE} \propto \sin 2\alpha$, the LPGE-induced photocurrent can be written in a form of $j_{LPGE} = j_{LPGE,1} \sin 4\alpha + j_{LPGE,2} \cos 4\alpha + j_{LPGE,3}$. The combination of these two photocurrents explains why we can write the emitted terahertz signals in a form of Eq. (3). (ii) We can readily find that when the incident laser pulse changes chirality from left-handed ($\alpha = \pi/4$) to right-handed ($\alpha = 3\pi/4$), the CPGE-induced photocurrent will change signs. Furthermore, the CPGE-induced photocurrent only flows along the direction perpendicular to the incident plane, which is consistent with the results in Fig. 3(d). (iii) From these four equations, we can qualitatively analyze the magnitude relationship of the photocurrent components. As in the x direction, from Eqs. (4) and (5), only CPGE-induced C_x and LPGE-induced L_{1x} components contribute to the photocurrent. Because the incident angle is relatively small, and L_{1x} contains the $\cos \theta$ term, L_{1x} should be significantly larger than C_x. And there is no L_{2x} contribution in the x direction. In the yz plane, C_{yz} and L_{1yz} are both 0, and the magnitudes of L_{2yz} and D_{yz} are approximately identical. The magnitudes of these current components determined by the crystal symmetry in the x axis and yz plane are in good agreement with the relative magnitudes of the various components extracted in our experiments except for D_x. There is a relatively large D_x, observed in experiment, and the physical origin of this component may come from a dark current,[30] which needs further investigation. (iv) It is worth noting that the PGE theoretical framework illustrates that photocurrent components all originate from the same PGE mechanism, which is exactly the evidence reflected by their frequency spectral shapes. Therefore, we can conclude that the phenomenological PGE mechanism framework determined by the symmetry of the crystal surface is adequate for explaining most of the salient features of the resulting photocurrents.

To acquire spin-polarized terahertz pulses with higher quality, we can also readily gain inspiration from the above framework. When the incident laser pulse is left-handed ($\alpha = \pi/4$), $j_{CPGE,x} = -2\gamma C^2 \sin \theta$, $j_{LPGE,x} = 0$, $j_{LPGE,yz} = f(\theta)$. When the incident laser pulse is right-handed ($\alpha = 3\pi/4$), $j_{CPGE,x} = 2\gamma C^2 \sin \theta$, $j_{LPGE,x} = 0$, $j_{LPGE,yz} = f(\theta)$. It indicates that when we change the chirality of the laser pulse, we can manipulate the polarity of the CPGE-induced photocurrent, keeping the

orthogonal component invariant. Based on this statement, we can further analyze the manipulation of phase and amplitude for terahertz radiation. As for the phase between the x axis and yz plane, two different physical processes actually exist. The physical process in LPGE represents a shift current along the Bi–Te bond. As for the process in CPGE, the laser with certain chirality will selectively excite a certain spin alongside the direction of incidence due to the spin texture of the surface states [Fig. 4(d)]. Subsequently, the asymmetry distribution of spin would result in a photocurrent that is perpendicular to the direction of the spin because of the spin-momentum locking.[26] As long as a phase difference between CPGE- and LPGE-induced photocurrents exists, which has already been assured by the above two different physical processes, spin-polarized terahertz radiation is guaranteed. Regarding the amplitude, randomly choosing incident angle θ cannot warrant indentical amplitude along the x axis and yz plane. This explains why we cannot achieve optimal ellipticity when employing circularly polarized pulses. Therefore, to optimize the ellipticity, we can increase the incident angle and look forward to achieving higher ellipticity in a wider spectrum.

In short, we systematically analyzed the features of L_1, L_2, and D via the symmetry on the surface of Bi_2Te_3 under a phenomenological PGE framework. We realized that the invariant L_2, D components, and polarity-controllable C component were all prerequisites for the spin-polarized terahertz emission. Furthermore, this framework can summarize most features of extracted components except for D_x and gives hints for achieving optimal spin-polarized terahertz emission, which owns significant guidance.

Based on the above theoretical analysis, we summarize the terahertz emission experimental results in Fig. 5. From these results, we can see that, for a fixed laser incidence angle, linearly polarized pump light can only produce linearly polarized terahertz waves [Figs. 2 and 5(c)], circularly polarized light can produce chiral terahertz waves, and its chirality is consistent with that of the pump laser [Figs. 5(a) and 5(b)]. To make the terahertz generation and manipulation more advanced, we can successfully realize various complex terahertz wave polarization shaping in topological insulators.

4 Conclusion

We systematically studied terahertz emission from topological insulator Bi_2Te_3 nanofilms driven by femtosecond laser oscillator pulses. Through experimentally investigating the sample thickness, azimuthal angle, and pump laser polarization-dependent terahertz radiation properties, we clarified that PGE played a predominant radiation mechanism in this light–matter ultrafast interaction process and produced efficient terahertz waves. Borrowing the spin-momentum–locked state-induced helicity-dependent spin-polarized current generation and combing it with the helicity-independent photocurrent, we not only realized circularly polarized terahertz beam generation but also demonstrated arbitrary manipulation of their polarization shaping in topological insulators via simultaneously adjusting the pump laser polarization states and sample azimuthal angles. Our method may have the feasibility to be extended to a variety of topological insulator materials and other related Dirac quantum materials. The topological insulator nanofilms can be grown with high quality and large size possible for high-field terahertz sources at transmission emission geometry, which may also provide very promising applications in fundamental nonlinear
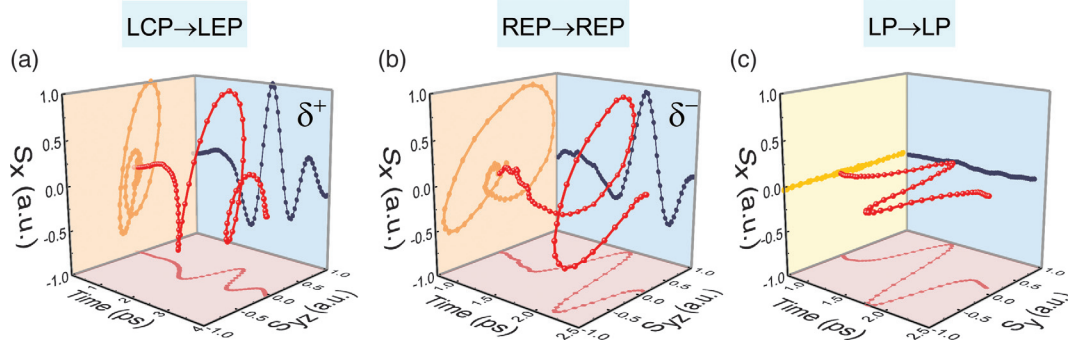
Fig. 5 Arbitrary manipulation of various terahertz polarization states. Radiated terahertz chirality was consistent with that of the pump laser chirality. (a) LCP pump laser pulses can produce left-handed elliptically polarized terahertz waves and (b) right-handed elliptically polarized pump light can generate right-handed elliptically polarized terahertz beams. (c) Linearly polarized terahertz waves can be generated in Bi_2Te_3 pumped by linearly polarized pump laser beams.

terahertz investigations and other real applications such as terahertz circular dichroism spectroscopy, polarization-based imaging, and terahertz secure communication.

5 Appendix: Methods

5.1 Appendix A: Sample Preparation and Characterization

Normal three-dimensional topological insulators are V to VI component semiconductors with a hexagonal crystal structure, in which the building block is a quintuple layer (QL). Our topological insulator nanofilms with 10-, 8-, and 5-nm thicknesses grown on 0.5-mm-thick sapphire are Bi_2Te_3 prepared by molecular beam epitaxy. As shown in Supplementary Note 1 and Fig. S1(a) in the Supplementary Material, each QL of Bi_2Te_3 consists of five atomic layers, terminating by Te atoms without dangling bonds, and a weak interaction called van der Waals force binds two neighboring QLs. This peculiar gap makes Bi_2Te_3 able to overcome the large lattice mismatch with sapphire substrates (~8%). Due to the weak adhesion between Bi_2Te_3 and sapphire, we employed a two-step deposition procedure. The initial 1 to 2 QLs of Bi_2Te_3 were deposited at a low temperature of 160°C. The lower temperature diminished the material quality, which promoted the stacking of atoms to the substrates. After finishing this first deposition, the substrate temperature slowly increased to 230°C. Based on these seed layers, the rest of the film could be deposited with a good quality.

5.2 Appendix B: Terahertz Emission Spectroscopy

In our experiment, we used a home-made terahertz time-domain spectrometer to carry out all of the measurements. The femtosecond laser pulses were from a commercial Ti:sapphire femtosecond laser oscillator with a central wavelength of 800 nm, a pulse duration of 100 fs, and a repetition rate of 80 MHz. About 90% of the laser energy was used for terahertz generation in topological insulators, and the residual was employed for electro-optic sampling in 1-mm-thick ZnTe detection crystal. Either a half-wave plate or a quarter-wave plate was inserted into the pumping beam before it illuminated onto the sample to vary the pump laser polarization states. The radiated terahertz pulses went through four parabolic mirrors and finally were

focused together with the probing beam into the ZnTe detector. Between the second and third parabolic mirrors, there were two terahertz polarizers inserted into the optical path to resolve the terahertz polarization.[19] The optical path from the terahertz emitter to the detector was sealed and pumped to eliminate the influence of water vapor. All of the experiments were carried out at room temperature.

5.3 Appendix C: Extracting Coefficients in Linearly and Circularly Polarized Terahertz Signals

According to Eq. (1), the basis functions $A(t)$, $B(t)$, and $C(t)$ are obtained by multiplying $S(t, \varphi)$ with $3/2\pi$, $3\sin(3\varphi)/\pi$, and $3\cos(3\varphi)/\pi$, respectively, and then subsequent integration from $\varphi = 0$ to $2\pi/3$. According to Eq. (3), the basis functions $C(t)$, $L_1(t)$, $L_2(t)$, and $D(t)$ are gained by multiplying $S(t, \alpha)$ with $2\sin(2\alpha)/\pi$, $2\sin(4\alpha)/\pi$, $2\cos(4\alpha)/\pi$, and $1/\pi$, respectively, and then subsequent integration from $\alpha = 0$ to π.

5.4 Appendix D: Retrieving Femtosecond Photocurrents

The measured electro-optic signal $S(t)$ and the terahertz electric field $E(t)$ near the sample surface have a linear relationship in the frequency domain as the following equation:

$$S(\omega) = H(\omega)E(\omega), \tag{8}$$

where $H(\omega)$ is the transfer function. After getting frequency domain $E(\omega)$, Ohm's law can be used to obtain the photocurrent $J(t)$ on the surface of Bi_2Te_3 as

$$J_x(\omega) = -\frac{\cos\theta + \sqrt{n^2 - \sin^2\theta}}{Z_0}E_x(\omega), \tag{9}$$

$$J_{yz}(\omega) = -\frac{n^2\cos\theta + \sqrt{n^2 - \sin^2\theta}}{Z_0\sqrt{n^2 - \sin^2\theta}}E_{yz}(\omega), \tag{10}$$

where θ is the incident angle, n is the refractive index of Bi_2Te_3 (shown in Supplementary Note 4 and Fig. S6 in the Supplementary Material), and $Z_0 \approx 377\,\Omega$ is the vacuum impedance. The photocurrent $J(t)$ can be gained from the

inverse Fourier transformation of the current spectra $J(\omega)$. More shapes of the physical parameters are shown in Supplementary Note 4 and Fig. S6 in the Supplementary Material.

Acknowledgments

References

1. S. D. Ganichev et al., "Spin-galvanic effect," *Nature* **417**, 153–156 (2002).
2. T. Kampfrath, K. Tanaka, and K. A. Nelson, "Resonant and nonresonant control over matter and light by intense terahertz transients," *Nat. Photonics* **7**, 680–690 (2013).
3. S. Zhang et al., "Photoinduced handedness switching in terahertz chiral metamolecules," *Nat. Commun.* **3**, 942 (2012).
4. M. Tamagnone et al., "Near optimal graphene terahertz non-reciprocal isolator," *Nat. Commun.* **7**, 11216 (2016).
5. T. J. Huisman et al., "Femtosecond control of electric currents in metallic ferromagnetic heterostructures," *Nat. Nanotechnol.* **11**, 455–458 (2016).
6. E. A. Mashkovich et al., "Terahertz optomagnetism: nonlinear THz excitation of GHz spin waves in antiferromagnetic FeBO$_3$," *Phys. Rev. Lett.* **123**, 157202 (2019).
7. T. N. Ikeda and M. Sato, "High-harmonic generation by electric polarization, spin current, and magnetization," *Phys. Rev. B* **100**, 214424 (2019).
8. W. J. Choi et al., "Terahertz circular dichroism spectroscopy of biomaterials enabled by kirigami polarization modulators," *Nat. Mater.* **18**, 820–826 (2019).
9. J. C. Boileau et al., "Robust quantum communication using a polarization-entangled photon pair," *Phys. Rev. Lett.* **93**, 220501 (2004).
10. C. Agnesi et al., "Simple quantum key distribution with qubit-based synchronization and a self-compensating polarization encoder," *Optica* **7**(4), 284–290 (2020).
11. N. K. Grady et al., "Terahertz metamaterials for linear polarization conversion and anomalous refraction," *Science* **340**(6138), 1304–1307 (2013).
12. M. Jia et al., "Efficient manipulations of circularly polarized terahertz waves with transmissive metasurfaces," *Light Sci. Appl.* **8**, 16 (2019).
13. A. G. Stepanov, J. Hebling, and J. Kuhl, "Generation, tuning, and shaping of narrowband, picosecond THz pulses by two-beam excitation," *Opt. Express* **12**(19), 4650–4658 (2004).
14. J. Y. Sohn et al., "Tunable terahertz generation using femtosecond pulse shaping," *Appl. Phys. Lett.* **81**, 13–15 (2002).
15. Q. Jin et al., "Preference of subpicosecond laser pulses for terahertz wave generation from liquids," *Adv. Photonics* **2**(1), 015001 (2020).
16. J. R. Danielson, N. Amer, and Y. S. Lee, "Generation of arbitrary terahertz wave forms in fanned-out periodically poled lithium niobate," *Appl. Phys. Lett.* **89**, 211118 (2006).
17. Z. L. Zhang et al., "Manipulation of polarizations for broadband terahertz waves emitted from laser plasma filaments," *Nat. Photonics* **12**, 554–559 (2018).
18. M. Sato et al., "Terahertz polarization pulse shaping with arbitrary field control," *Nat. Photonics* **7**, 724–731 (2013).
19. D. Y. Kong et al., "Broadband spintronic terahertz emitter with magnetic-field manipulated polarizations," *Adv. Opt. Mater.* **7**(20), 1900487 (2019).
20. X. H. Chen et al., "Generation and manipulation of chiral broadband terahertz waves from cascade spintronic terahertz emitters," *Appl. Phys. Lett.* **115**, 221104 (2019).
21. N. Kanda et al., "The vectorial control of magnetization by light," *Nat. Commun.* **2**, 362 (2011).
22. Y. Gao et al., "Chiral terahertz wave emission from the Weyl semimetal TaAs," *Nat. Commun.* **11**, 720 (2020).
23. X. B. Wang et al., "Ultrafast spin-to-charge conversion at the surface of topological insulator thin films," *Adv. Mater.* **30**(52), 1802356 (2018).
24. H. Plank et al., "Photon drag effect in $(Bi_{1-x}Sb_x)_2Te_3$ three-dimensional topological insulators," *Phys. Rev. B* **93**, 125434 (2016).
25. C. M. Tu et al., "Helicity-dependent terahertz emission spectroscopy of topological insulator Sb$_2$Te$_3$ thin films," *Phys. Rev. B* **96**, 195407 (2017).
26. J. W. McIver et al., "Control over topological insulator photocurrents with light polarization," *Nat. Nanotechnol.* **7**, 96–100 (2012).
27. S. Y. Hamh et al., "Helicity-dependent photocurrent in a Bi$_2$Se$_3$ thin film probed by terahertz emission spectroscopy," *Phys. Rev. B* **94**, 161405 (2016).
28. H. J. Zhang et al., "Topological insulators in Bi$_2$Se$_3$, Bi$_2$Te$_3$ and Sb$_2$Te$_3$ with a single Dirac cone on the surface," *Nat. Phys.* **5**, 438–442 (2009).
29. Z. J. Fang et al., "Nonlinear terahertz emission in the three-dimensional topological insulator Bi$_2$Te$_3$ by terahertz emission spectroscopy," *Appl. Phys. Lett.* **115**, 191102 (2019).
30. Y. Pan et al., "Helicity dependent photocurrent in electrically gated $(Bi_{1-x}Sb_x)_2Te_3$ thin films," *Nat. Commun.* **8**, 1037 (2017).
31. L. Braun et al., "Ultrafast photocurrents at the surface of the three-dimensional topological insulator Bi$_2$Se$_3$," *Nat. Commun.* **7**, 13259 (2016).
32. P. Olbrich et al., "Room-temperature high-frequency transport of Dirac fermions in epitaxially grown Sb$_2$Te$_3$- and Bi$_2$Te$_3$-based topological insulators," *Phys. Rev. Lett.* **113**, 096601 (2014).
33. G. Gallot et al., "Measurements of the THz absorption and dispersion of ZnTe and their relevance to the electro-optic detection of THz radiation," *Appl. Phys. Lett.* **74**, 3450–3452 (1999).
34. J. Yu et al., "Helicity-dependent photocurrent of the top and bottom Dirac surface states of epitaxial thin films of three-dimensional topological insulators Sb$_2$Te$_3$," *Phys. Rev. B* **100**, 235108 (2019).
35. M. Chen et al., "Anisotropic picosecond spin-photocurrent from Weyl semimetal WTe$_2$," *ACS Nano* **14**(3), 3539–3545 (2020).
36. P. H. Le et al., "Thickness-dependent magnetotransport properties and terahertz response of topological insulator Bi$_2$Te$_3$ thin films," *J. Alloys Compd.* **692**, 972–979 (2017).
37. D. L. Mills, *Nonlinear Optics: Basic Concepts*, Springer Science & Business Media (2012).
38. A. Junck, "Theory of Photocurrents in Topological Insulators," PhD Thesis, im Fachbereich Physik der Freien Universitat Berlin eingereichte (2015).

Haihui Zhao is a graduate student at Beihang University. She received her bachelor's degree from the School of Electronic and Information Engineering of Beihang University in 2019. She joined Professor Xiaojun Wu's and Professor Tianxiao Nie's terahertz group in September of 2019. Her research interest is focused on terahertz emission physics from new materials, such as magnetic materials and 2D materials.

Xinhou Chen is a graduate student at Beihang University in Xiaojun Wu's group. His main research interests are terahertz generation and manipulation. Currently, he focuses on chiral terahertz wave generation by combining spin-to-charge conversion and PGE in topological insulator.

Chen Ouyang is a PhD student at the University of Chinese Academy of Sciences. He is currently conducting research on the interaction of strong field terahertz with matter in Yutong Li's research group in the Key Laboratory of Optical Physics, the Institute of Physics, Chinese Academy of Sciences. He also received a bachelor's degree in physics from Beijing Institute of Technology in 2017.

Hantian Wang is a PhD student at Beihang University. He received his bachelor's degree in electrical information engineering from Zhengzhou University in 2017. In September 2017, he joined the Microelectronics Department of Beihang University, pursuing his PhD under the supervision of Professor Tianxiao Nie. His current research topics involve the growth of topological insulators and related heterostructures using MBE. He is also interested in ultrafast spin dynamics and spin terahertz emission.

Xiaojun Wu graduated with a PhD from the Institute of Physics, Chinese Academy of Sciences, in 2013. During August 2014–April 2017, she was awarded the Alexander von Humboldt Fellowship and joined in Professor Franz X. Kaertner's group at DESY in Germany. She became an associate professor in Beihang University in June of 2017 and is now an associate editor of *Optics Express*. She has published 80 academic papers in top journals and given more than 30 keynote and invited talks in international optical and terahertz conferences. She also served as co-chair or committee member for IRMMW-THz, OTST, FiO, and CLEO. Her research interests include generation of high-energy terahertz radiation and its extreme science and applications, terahertz emission physics from new materials, and on-chip terahertz photonics.

Biographies of the other authors are not available.